Optical and Quantum Electronics (2024) 56:262
https://doi.org/10.1007/s11082-023-05845-y

Optical fiber dual-parameter sensors based on different kinds of interferometers for measuring refractive index and temperature: a review

Chunfei Duan[1] · Jin Li[1,2] · Kai Zhang[1] · Mingjun Tian[1]

Received: 2 June 2023 / Accepted: 15 November 2023 / Published online: 27 December 2023

Abstract

Temperature and refractive index are two important parameters for many fields, where their accurate measurement is crucial. This review discusses the development of refractive index and temperature dual-parameter fiber sensors based on different interferometric structures in recent years, such as the Mach–Zehnder, Michelson or Fabry–Perot interferometers, which are composited by the grating reflectors, and multi-separated-region based on thin film layers and special structures. The working principle and performance of different types of sensors are analyzed. This review can provide the technical references for the development of novel dual-parameter sensors with practical potential and high performance.

Keywords Optical fiber sensors · Refractive index sensor · Temperature sensor · Dual-parameter measurement · Optics integration

1 Introduction

In the research fields of high-speed communication, high-precision sensing, optics precise-modulation, and photonics integration, the technological breakthroughs in performance improvement and cost reduction of optical devices have always been existing as the key issues(Sharma et al. 2018). Optical fiber sensors have been widely considered due to their small size, high sensitivity, and resistance ability to electromagnetic interference. With the

✉ Jin Li
lijin@ise.neu.edu.cn

Chunfei Duan
1498980179@qq.com

Kai Zhang
1941780474@qq.com

Mingjun Tian
1106959462@qq.com

1 College of Information Science and Engineering, Northeastern University, Shenyang 110819, China

2 College of Mechanical and Electronic Engineering, Northwest A and F University, Yangling 712100, China

gradual improvement of processing methods and the continuous enrichment of sensitive materials and micro/nano-structures, optical fiber sensors have revealed their promising potential applications in intelligent industry, life health, environmental protection, energy production and transportation, structural health and national defense security(Lu et al. 2019; Li et al. 2022; Wang et al. 2020a). The flexible design process for various fiber structures based on new materials have been enriching the development of novel optical sensors with excellent performance(Guo et al. 2022a). The combination of refractive index and temperature two-parameter measurement can provide more comprehensive information, so the development of temperature and refractive index two-parameter optical fiber sensor has attracted much attention.

In this review, the refractive index (RI) and temperature dual-parameter sensors based on optical fiber interferometers have been reviewed. The sensing performance of typical structures has been analyzed and compared in detail. We will focus on discussing the sensor structures and related performance for the relative widely used demodulation methods, such as wavelength and intensity, to analyze and compare the sensing performance of the reported works in recent years. This paper also discusses the related technologies to improve the performance of RI and temperature dual-parameter fiber sensors in the case of morphological separation of the sensing region, as well as the development of various novel optical sensors based on new materials.

2 Some basic fiber structures used for developing complex interferometers

Mach–Zehnder Interferometer (MZI) and Michelson Interferometer (MI) are both optical interferometric devices used for measuring the phase difference or wavelength of light. They differ in several aspects: configuration, interferometric principle, and application field. In details, MZI splits a beam of light into two beams using a beam splitter and introduces a sample beam and a reference beam into the respective paths of these two beams before recombining them for interference. MI, on the other hand, splits a beam of light into two beams using a partially reflective mirror and then reflects these two beams along different paths before recombining them for interference.

MZI utilizes the phase difference between the measure and reference beams to produce the interference phenomena and detect some parameters, such as refractive index or thickness. MI, however, obtains the interference phenomena by changing the length difference for its multi-paths, enabling measurements of parameters like light velocity, wavelength, and refractive index. Due to their different configurations and interferometric principles, MZI is commonly used for measuring the thickness of films, refractive index of transparent materials, etc. MI, on the other hand, finds applications in measuring the speed of light, precise length, and other related areas. The output intensity of an MZI and MI can be expressed mathematically as formula 1 and formula 3, where, I is the output intensity, I_0 is the average intensity, T_1 and T_2 are the transmission coefficients of the two arms of the MZI, R_1 and R_2 are the reflection coefficients of the two mirrors in the MI. $\Delta\varphi$ is the phase difference between two paths.) The phase difference $\Delta\varphi$ is given by formula 3, where, λ is the wavelength of the light, L is the length of the arms, n_1 and n_2 are the refractive indices of the two arms. In Formula 4, λ is the wavelength of the light, d is the difference in the lengths of the two arms, n is the refractive index of the medium.

$$I = I_0 + 2\sqrt{T_1 T_2} \cos(\Delta\phi) \quad (1)$$

$$\Delta\phi = \frac{2\pi L(n_2 - n_1)}{\lambda} \quad (2)$$

$$I = I_0 + 2\sqrt{R_1 R_2} \cos(\Delta\phi) \quad (3)$$

$$\Delta\phi = \frac{4\pi d (n - 1)}{\lambda} \quad (4)$$

In the Mach–Zehnder interferometer (MZI) and Michelson interferometer (MI) structures, the light beam was divided into two parts, which will travel in different optical paths and play as the reference and information signals, respectively, and produce the optical interference phenomenon. Usually, the two parts light signals can be acted by the core and cladding modes, as well as the fundamental (lower-order) and higher-order modes. The modes interference is produced in different fiber structures prepared or composited by the mode field mismatched splicing, dislocation splicing, diameter abrupt, bending, and gratings. The RI change directly exerts an impact on the intensity distribution of cladding modes; due to the thermal expansion effect as a function of temperature fluctuation, the propagation constant of light signal will change. Either RI or temperature effects on the corresponding parameters of interference spectrum, thereby establishes the physical relationship between the measured parameters and the light parameters (phase, wavelength, intensity, mode field, etc.).

MIs provides simultaneous measurement of two parameters with a single device. They have a larger dynamic range and are less sensitive to environmental factors such as vibration or temperature fluctuations. However, MIs are more complex to manufacture and arrange, and their sensitivity to each parameter can be affected by others, resulting in crosstalk. MZIs are highly sensitive to changes in one parameter and insensitive to changes in another parameter. Therefore, MI are more suitable for two-parameter measurement.

The Fabry–Perot interferometer (FPI) is also used to produce interference phenomena. It consists of two parallel partial mirrors that form an air gap or medium between them (also named as one Fabry–Perot cavity). In the FPI structures, parallel incident lights are reflected and transmitted several times in the cavity between the two reflected mirrors. These reflected and transmitted beams interfere with each other, forming a series of interference peaks and valleys. The interference peak corresponds to the region with the greatest light intensity, while the interference valley corresponds to the region with the least light intensity.

2.1 Mode field mismatched splicing fiber structures

When the optical fibers with different diameters are spliced together, the light will be split to multiple beams at the splicing point. They will re-couple at the next splicing point and produce an interference spectrum. These fiber structures usually refer to the cascade-spliced fibers by insert-splicing one fiber with different diameter (such as the multi-mode fiber (MMF), few-mode fiber (FMF) or coreless fiber (CLF)) among the single-mode fiber (SMF) system. During the splicing process, the fiber cores for the different fibers are generally coaxially aligned and cascade-spliced by an optical fiber fusion splicer. The coupling efficiency among different optical fibers depends on their special structures.

The spliced fiber structures are designed to build the compact MZI, including MMF-FBG-MMF(Hu et al. 2016), ultra-thin core fiber (uTCF)-TCF-uTCF(Liu et al. 2020) and FMF/MCF-SMF-FMF/MCF(Zuo et al. 2021).Their schematic diagrams are shown in Fig. 1a, b and c, respectively, in which the intermodal interference spectra based on the core (lower-order) modes and cladding (higher-order) modes are obtained at the splice points(Wang et al. 2016). The sensing performance for the excited cladding modes differs to each other for the inserted fibers with different unique morphological structures. FBG refracts most of the light outside the fiber core, and the metal film coated on the surface of the fiber is sensitive to the light signal, resulting in the sensitive performance for temperature and refractive index. For uTCF, the optical signal mainly transmits inside the cladding mode, which has a high sensitivity for RI because it can directly contact with the external environment to receive the changing information. With the change of temperature, the thermal expansion coefficient of the fiber material changes, as well as for the optical path difference, which leads to the wavelength drift of the spectrum.

The sensing performance for these sensors can be optimized in terms of geometric parameters, such as fiber types (special fibers with different structures) and spliced length (sensing regions with different lengths). For example, several segments of MMFs with different lengths were used to fabricate the multi-interferometer (with different interfering phases) series structures (Tong et al. 2014). Similarly, different cascade-fibers were designed for the multi-point measurement for different regions or targets(Chen et al. 2015a). The transmitted light signal is usually the multi-set superposition of interference spectra from the different sub-interferometer (Mohammed et al. 2004). In addition to launching the optical signal out from the core to produce the higher-order

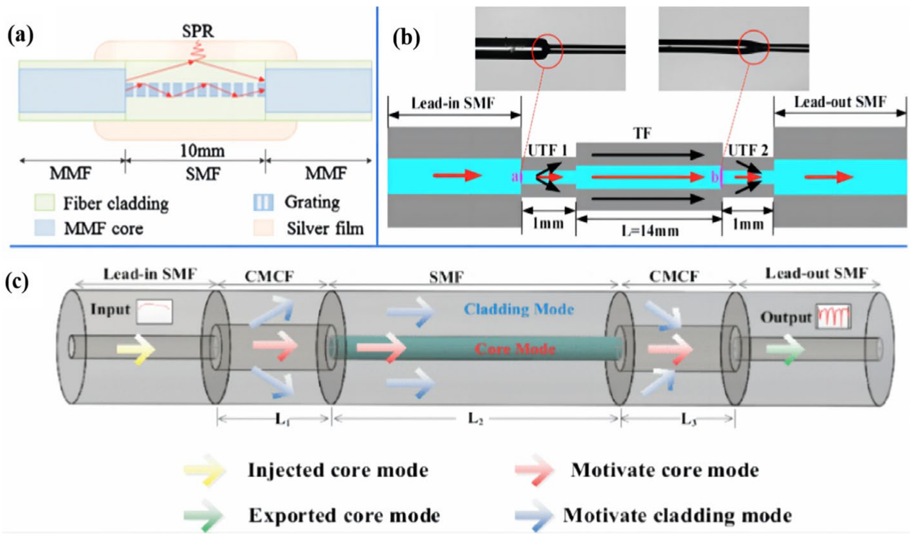

Fig. 1 Typical mode field mismatched splicing structures including MCF (Hu et al. 2016), uTCF (Liu et al. 2020) and FMF (Zuo et al. 2021)

modes in the cladding layer, the super mode interference can be generated among the core modes for an MMF, which can be realized by the cascade-splicing SMF and MMF (Flores-Bravo et al. 2021).

2.2 Dislocation splicing fiber structures

It is also possible to guide part of optical signal out from the fiber core in the asymmetric structures, which can be prepared by dislocation splicing, melting-tapering and melting-pushing. These asymmetric structures can effectively enhance the interference effect between high-order and low-order modes. Dislocation splicing structures are designed and fabricated by prior-offsetting the fiber core before the splicing operation, also known as core-offset splicing. The simplest dislocation splicing structure only contains the traditional SMF (Yao et al. 2014), as shown in Fig. 2a. This dislocation splicing structure can be fabricated by an optical fiber fusion splicer by reasonably setting the dislocation parameters and discharge intensity. At the offset splicing point, light beam is divided into two parts, which are left in the core and launched into the cladding layer (generating the cladding mode), respectively. The cladding modes re-couples into the fiber core after traveling through the sensing area, finally interfering with the core modes to produce the interference spectrum. However, the interference effect is not obvious due to the significant light intensity difference between the different modes.

All-fiber MZI can be flexibly designed based on the dislocation splicing structures and optimized by inserting a cut of SMF, MCF or MMF as the sensing area between two standard SMFs (Table 1).

2.3 Diameter changing fiber structures

During the heating and stretching process of SMF, the diameter can be continuously reduced to produce the biconical microfiber taper. Because of the micro-scale morphology in tapering region, the optical field will escape from the fiber core and enter into or even outside from the cladding layer in the form of optical evanescent waves. When The core diameter for the ordinary SMF (5 ~ 8 μm) becomes close to the working wavelength, the light leakage will be exacerbated. The corresponding sensing mechanism can be explained by the optical evanescent field theory of micro/nanofiber sensors. The evanescent fields can be easily obtained in a uTCF with very thin core, but it will be difficult for the biconical

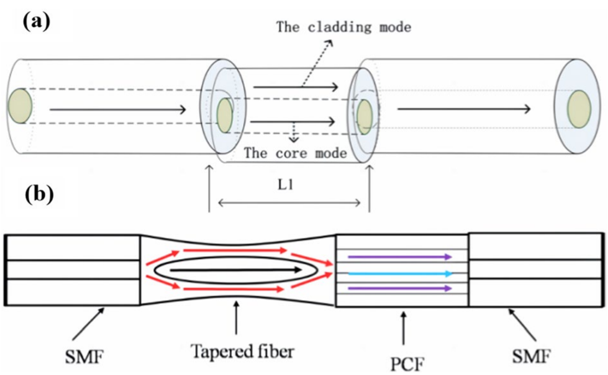

Fig. 2 Schematic diagram **a** dislocation-splicing(Yao et al. 2014), and **b** diameter reducing(Ni et al. 2016a) structures fiber sensors

Table 1 Performance comparison of two-parameter sensors based on interferometers

Structure type	RI sensitivity (nm/RIU)	Temperature sensitivity (pm/℃)	RI range (RIU)	T range (℃)	Refs
Mode field mismatched splicing fiber structures	2556.8	172	1.33–1.38	30–65	6
	− 169.0879	46.4	1.4578–1.444	25–75	7
	− 76.88	80.2	1.333–1.373	0–70	8
	86.7434	59	1.3105–1.3517	25–85	9
	100.97	138.5	1.3400–1.3900	20–70	10
	113.66	9.2	1.333–1.376	30–95	11
Diameter changing fiber structures	3820.23	− 465.7	1.3315–1.3350	30–60	15
	55.84	143	1.3400–1.4400	20–70	16
	111.14	131	1.3400–1.3800	20–70	17
	− 35.0502	145.6	1.3476–1.4285	30–95	18
	− 27.77	54	1.335–1.398	25–80	19
	464.96	28.7	1.3631–1.3812	35–85	20
Bending fiber structures	− 1705.66	134	1.3330–1.3581	30–75	21
	1191.5	64.8	1.3405–1.3497	20–90	22
	167.309	35	1.3400–1.3805	25–75	23
	331.71	− 1053	1.333–1.404	30–70	24
	245	250	1.3403 – 1.3726	13–36	25
	108.61	19	1.3355–1.3758	25–85	26

MMF with relatively bigger size, in which the optical signal transmits inside the fiber core by total internal reflection. However, the leakage light near the biconical region produces a relatively high sensitivity to RI and temperature change (up to 3820.23 nm/RIU, −465.7 pm/℃) (Luo et al. 2015). The mechanism can be explained by the multi-beam splitting and interfering similar in the MZI fiber structures. The multi-beam interference can also be achieved in a tapered air cavity(Ni et al. 2016a), as shown in Fig. 2b, which is prepared by introducing the air near the fusion end-faces during the melting-tapering process. The structural parameters of the rugby-shaped air cavity are difficult to adjust, relying on the precise positioning and splicing. The biconical tapered microfiber plays an important role for the light transmission and beam size change, that is to reshape the optical mode field in the SMF core and launch it into the cross-section with special fiber microstructures of PCF.

Conversely, the bigger diameter is prepared under the radial extrusion force. Its morphology can be finely adjusted by the intensity, timing and location of the arc discharge in a fusion splicer. The cladding modes can be efficiently excited into the fiber structure with bigger diameter. The cascade-splicing of multi-fiber with bigger diameter can realize the efficient coupling between the cladding modes and the core modes in the cross-section, or the reflected light interference by the split multi-beam. Dislocation-splicing structures can also be introduced to collect the core and cladding modes, so as to improve the interference efficiency. Different from the biconical microfiber sensors, the structure with bigger diameter extends the sensing area from the middle part (tapering region with a decreasing diameter) to the whole connecting region covering the bigger diameter region and its nearby middle part, where the separation point and coupling point for the interferometer become clearer(Su et al. 2014). The inserted fiber can be flexibly replaced and optimized to achieve the desired polarization state (polarization mode fiber, PMF) (Zhao et al. 2017a) or number of modes (FMF and MMF) (Tong et al. 2018). In addition, the diameter increasing structure was polished to obtain a biconical microfiber structure containing a pair of spherical air cavities to enhance the interaction efficiency between optical signals and external environment (Liu et al. 2016a). The RI sensitivity was reported to be 464.96 nm/RIU.

2.4 Bending fiber structures

Bending fiber structure can destroy the total reflection condition and leak the optical signal into the cladding layer of optical fiber. Due to the different propagation constants between the cladding and core modes, the optical path difference will be generated and result in the mode interference. The U-shaped or balloon-shaped bending fiber is equivalent to an MZI or MI.

To construct a compact U-shaped interferometer with stable structure, the internal stress of the uncoated bare fiber should be released using the heating process. The alcohol lamp was used to reduce the bending radius to 500 μm(Ge et al. 2020). The RI sensitivity and Temperature sensitivity reach −1705.66 nm/RIU and 134 pm/℃. Commonly, the U-shaped bending region should be long enough to insert in other fibers or special structures (biconical microfiber, MMF, CLF, dislocation splicing point, etc.). In this way, a dual-MZI structure is constructed for simultaneous measuring RI and temperature(Wang et al. 2020b), as shown in Fig. 3a. The first MZI is built by the mode field mismatch splitter by inserting different fibers, while the second MZI was played by the bending fiber structure. Figure 3b shows the sequential cascade-structure based on different types of fibers, including SMF, biconical-bending MMF, and CLF(Zhao

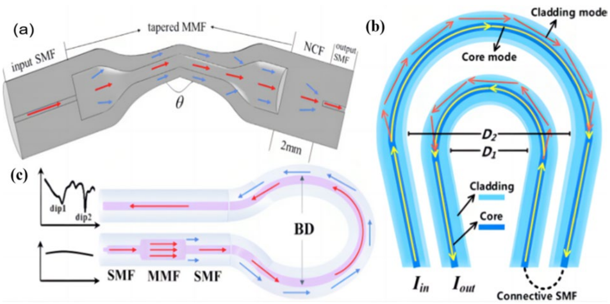

Fig. 3 Schematic diagram of typical bending fiber sensors based on **a** folded-tapered multimode-CLF(Wang et al. 2020b), **b** multiple cascade-fibers(Zhao et al. 2018) and **c** nested balloon-ring(Hu et al. 2020) structures

et al. 2018). Where, the core mode in SMF is excited into various propagation modes in MMF; the cladding mode is excited at the bending structure of MMF and interferes with the core mode in CLF; the final interference is produced at the output SMF. The high RI sensitivity can be obtained due to the strong optical evanescent wave around the biconical microfiber. Figure 3c illustrates a nested balloon-ring fiber structure(Hu et al. 2020), which was designed by splicing MMFs in a SMF system to launch part of the light signal into cladding layer before the bending fiber structure. It effectively increases the transmission length of the cladding modes in the bending regions, that is, the length of the whole sensing region became longer.

Similarly, the sensing length can also be extended by concatenating different bending fiber structures(Zhang and Peng 2015). During the measurement process, the RI information of the surrounding environment will exert the more significant impact on the transmission light. By cascading two MZI structures with different performance, the crosstalk effect between RI and temperature measurement will be reduced, so as to improve the sensing accuracy. For example, a novel anti-resonant reflection waveguide was proposed by cascaded-splicing the capillaries with SMFs, and series-connecting it within a bending fiber ring structure(Zheng et al. 2022) for simultaneous measurement of RI and temperature. The loss dip of the anti-resonant reflective waveguide was used as reference to supply the compensation for the ambient temperature fluctuations(Sun et al. 2020; Liu et al. 2016b).

3 In-line fabry–perot interferometers

Fabry–Perot interferometer (FPI) is suitable for designing RI and temperature dual-parameter sensors attributed to three reasons: (1) FPI sensor relies on the cavity length variation as a function of the target parameter changes, resulting in its large working range (especially for temperature); (2) FPI can be integrated in the SMF system by means of middle-inserting or end-face constructing. Multiple FPIs can be easily fabricated by continuously cascade-splicing some small segments of fibers or air cavity with flatted reflectors; (3) It has the high-stable structure and mature demodulation technique(Wu et al. 2015). The phase change of the FPI spectra can be demodulated by the Fourier transformation method. The output intensity of an FPI is shown in Formula 5, where, I is the output intensity, I_0 is the average intensity, F is the finesse of the FPI, R_1 and R_2 are the reflection coefficients of the two mirrors in the FPI, δ is the optical path difference between the two arms of the FPI, λ is the wavelength of the light.

$$I = I_0 * \left(1 + F * \cos\left(\frac{2\pi\delta}{\lambda}\right)\right)^2 \quad (5)$$

$$F = \pi\sqrt{\frac{R_1R_2}{1 - R_1R_2}} \quad (6)$$

An FPI-based dual-parameter sensor for measuring RI and temperature is usually designed by connecting two FPI structures with an open and closed cavity, respectively. Where, the former open cavity directly contacts with the external environment, in which both RI and temperature of either liquid or gas filled in the Fabry–Perot (FP) cavity will affect its interference phase; the latter closed cavity with the solid structure is independent on the RI of environmental medium. Its cavity length will be only affected by the ambient temperature. These two FP cavities are different in their lengths to produce two sets of interference spectra with different frequency and realize the simultaneous detection of RI and temperature. By dislocation-splicing the thin fiber with a standard SMF with large off-center alignment, an open FP cavity can be constructed(Ni et al. 2016b). The closed air cavity can also be prepared by etching the air hole at the end-face of fiber, such as the graded-index few-mode fiber in Fig. 4a, where a miniature cavity was fabricated and used as microfluidic refractometer(Fu et al. 2020). The RI sensitivity and Temperature sensitivity reach − 16.03 dB/RIU and 10.52 pm/℃. Temperature compensation can make the refractive index accurate, but the temperature sensitivity is low, in the case of relatively high temperature requirements, this structure is not suitable.The fiber end-face was etched to be an air microcavity by hydrofluoric (HF) acid. It was further-spliced with SMF, leaving its another end-face as a flat reflector. In this probe, two FPIs refer respectively to the air microcavity structure (with two reflectors at wall-interface) and the segment of the few-mode fiber (with two reflectors at end-face).

In addition to the chemical etch method, the FP microcavity can also been precisely designed by the laser machining technique based on femtosecond laser or CO_2 laser. The open FP microcavity is obtained by chiseling through SMF, while the solid

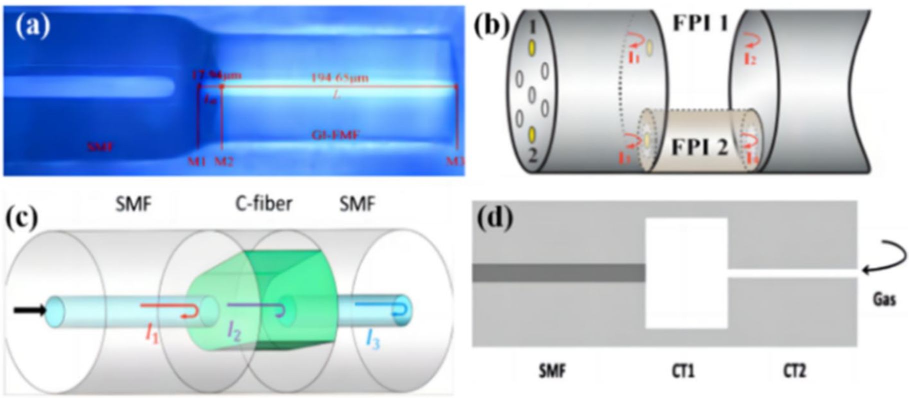

Fig. 4 Schematic diagram of FPI dual-parameter fiber sensors based on **a** graded-index few mode fiber(Fu et al. 2020); **b** multi-core splitter(Ouyang et al. 2018), **c** C-shape cavity (Li et al. 2020) and **d** capillary-cavity structure(Wang and Qiao 2014)

FP cavity is obtained by flat-cutting two end-faces reflectors on common SMF, finally forming a double-microcavity cascade FPIs structure(Ran et al. 2013). Combining the intensity and phase modulation technique for the FP interference spectra, the RI and temperature were simultaneously measured by detecting the fringe contrast (V) and the interference phase shift, respectively. In the cascaded-FPIs structure for RI and temperature sensing, the FP air microcavity for RI detection is prepared during the fusion splicing process between the two end-faces of various fibers, such as SMF and MMFs(Zhao et al. 2015; Shi et al. 2015), etc.; polymers (sol gel) are also ideal materials for making FP microcavities by encapsulating a certain of air inside a capillary to fabricate the air cavity(Zhang et al. 2013).

The Vernier effect based on the two interferometers with little different interfering length provides the new ideas and possibilities for developing the dual-parameter sensors(Jiang et al. 2022a). Furthermore, two more interferometers can produce the composite Vernier effect. The PMF-SI was parallel-connected with the solid FPI to generate the first Vernier effect. It was then parallel-connected with the open-cavity FPI to obtain the second Vernier effect. The superimposed spectrum of the two Vernier effects is called composite Vernier spectrum. By monitoring the phase shift of its upper and lower envelopes, the RI and temperature sensitivities were experimentally obtained to be − 19,844.67 nm/RIU and − 46,140 pm/℃, respectively.

In an all-fiber micromechanical sensor, two fiber internal mirrors are designed to form a solid FPI by preparing RI abrupt points in the fiber core of a SMF(Pevec and Donlagic 2014). This fabrication process is very similar to write the Bragg gratings in the fiber core. The difference is that the RI abrupt points have a bigger size and are fabricated at two locations. The open-cavity FPI was fabricated by HF-etching the P_2O_5-doped-CLF and splicing it further with the solid FPI. The parallel-structured fiber FPI was used as a temperature-compensated refractometer(Ouyang et al. 2018). By splicing a piece of HCF between the seven-core fiber and SMF, two mutually independent open and closed FPIs are obtained, as shown in Fig. 4b. Where, the open cavity provides the interaction relationship between the environmental parameters and transmitted light. Closed cavities are only sensitive to temperature. This dual-FPI structure is realized by simple splicing process. Similarly, a dual-FPI temperature-compensated refractometer based on C-shape fiber is designed(Li et al. 2020), as shown in Fig. 4c. Two cascaded FPIs based on C-shape fiber has been made from the silica capillary with side grooves (marked in green color), in which the liquid is filled and flows.

Table 2 Sensing performance comparison of dual-parameter sensors based on FPI

RI sensitivity (nm/RIU)	Temperature sensitivity (pm/℃)	RI range (RIU)	T range (℃)	Refs
− 16.03(dB/RIU)	10.52	1.3331–1.3568	30–90	31
44.9(dB/RIU)	0.02 (dB/°C)	1.0–1.42	50–380	32
− 67.9 (dB/RIU)	− 92.6	1.33–1.38	28–51	33
57.24 (dB/RIU)	10	1.3415–1.4320	30–70	34
− 240.425 (dB/RI)	385.46	1.3625–1.4150	25–60	35
− 19,844.67	− 46.14	1.333–1.339	27–30	36
1096.6	− 137.6	1.3435–1.3677	20–80	38
1704	− 196	1.3162–1.3303	25–45	39

In-line Fabry–Perot interferometers are compact and versatile optical devices that utilize interference patterns for precise measurements. They offer high sensitivity and can operate over a wide range of wavelengths. However, they are sensitive to environmental factors and may have limitations in achieving high finesse. Overall, they are valuable tools in various optical applications, providing a balance between simplicity and accuracy (Table 2).

Above two structures have the different FPIs (parallel or series connecting), which both contain an open-cavity and a solid fiber. The sensing performance and fabrication process for the two FPIs are different to each other. C-shape fiber provides a large detection cell to ensure the detection efficiency for RI and temperature of fluid. Furthermore, the same diameter and large connecting region compared to SMF can effectively improve the structural stability.

To reduce the cost, the cascade-splicing SMFs with large dislocation can also be used for the simultaneous measurement of RI and temperature (Zhou et al. 2021). The dislocation value should be greater than the fiber radius of the SMF to form the open-cavity structures. The high RI sensitivity has been experimentally demonstrated to be 1084 nm/RIU. A hybrid fiber FPI for simultaneous measurement of gas RI and temperature was designed(Wang and Qiao 2014) in Fig. 4d. Where, two capillaries with different inner diameters have been cascaded-spliced. An external FPI is formed in the air gap cavity based on the large diameter capillary. Another segment of capillary with a smaller inner diameter serves as an intrinsic FPI and also provides a channel for the gas flowing and exchanging.

4 Optical fiber interferometers based on gratings reflectors

Different gratings in optical fibers can be used as the special reflectors (or filters) to develop the FPI (or MZI) fiber interferometers. Fiber Bragg grating (FBG) is mainly used to induce the back-coupling of co-transmission core modes, whose characteristic wavelength is dependent on the change of either the grating period (due to the stretching force along the fiber) or the effective RI of fiber core change (due to the thermal induced expansion caused by temperature change)(Guo et al. 2022b). Long-period fiber gratings (LPFGs) promote the in-direction mode coupling effect between the core modes (fundamental modes) and the cladding modes (higher-order modes). The grating structure and the fiber cross section of the tilted FBG (TFBG) is tilted with an angle of several degrees (usually 8 degrees), which can effectively couple the forward propagating mode with one or more backward propagating cladding modes. The mode coupling in these kinds of fiber gratings (FBG, LPFG and TFBG) contains different light modes, and have been widely concerned in developing the novel multifunctional fiber sensors.

Optical fiber interferometers based on grating reflectors offer high precision, sensitivity, reliability, and strong resistance to interference. However, they can be expensive, require stable light sources and high-quality fibers, and involve complex signal processing. Consideration of these factors are essential when choosing and applying this type of interferometer.

4.1 Fiber grating pairs used as reflectors

The FBG and LPFG can be obtained, respectively, by etching the periodic grating structures in the fiber core (by UV laser mask-etching or femtosecond laser direct-writing technology) and on the cladding outer-surface (by CO_2 laser thermal-melting technique). The gratings in the period of micrometer scales are more sensitive to temperature changes, where the different periods results in the change of interference wavelength and the wavelength shift of characteristic peak. This phenomenon contributes the sensing mechanism due to the thermal expansion effect of the materials for different temperatures. The RI sensing of FBGs can be realized by fixing the polymer materials outside the fiber to convert the RI change to be the radial stress along the gratings region. While, for the LPFG, its characteristic wavelength is directly dependent on the RI of ambient environment. In terms of temperature sensing, the sensitivity of FBG depends on the coefficient of thermal expansion and the spectral characteristics of fiber grating. The thermal expansion coefficient refers to the dimensional change rate of the material with temperature, and the spectral characteristic refers to the reflection or transmission spectrum of the grating with temperature.

The preparation methods of FBG mainly include the UV mask-etching and laser direct writing ways. During the directly writing process of FBG, the femtosecond laser beam transmits through the transparent cladding layer and is focused on the fiber core at precise positions with a small focus radius, which greatly improves the processing accuracy and high temperature adaptability for the FBG structures compared to the UV mask-etching method(Lacraz et al. 2015; Bernier et al. 2014). The environmental RI and temperature fiber sensor has been reported based on unclad-FMF-FBG structure(Gunawardena, et al. 2015). The chemical etching method was used to remove the FMF's cladding layer and expose the FBGs region, producing the coupling effect among the multiple light beams, including the core (fundamental) mode, cladding (higher-order) modes, and evanescent field modes. The coupling parameters are simultaneously affected by ambient RI and temperature changes, resulting in the characteristics peaks shift in the superimposed spectra. Therefore, the sensitivities of 4.816 nm/RIU and 9.57 pm/℃ can be obtained for RI and temperature, respectively. In addition to reducing the diameter to excite cladding modes and optical evanescent fields, the bending FBG structure has also been reported to construct a RI sensing region(Liu et al. 2016c), as shown in Fig. 5a. The whispering gallery modes (high-order modes) excited in the cladding layer of the bending fiber region were coupled with the core modes in FBGs. It will produce different characteristic resonance wavelengths in the transmission spectrum. The sensitivities are determined to be 165.9276 nm/RIU and 31.7 pm/℃, respectively.

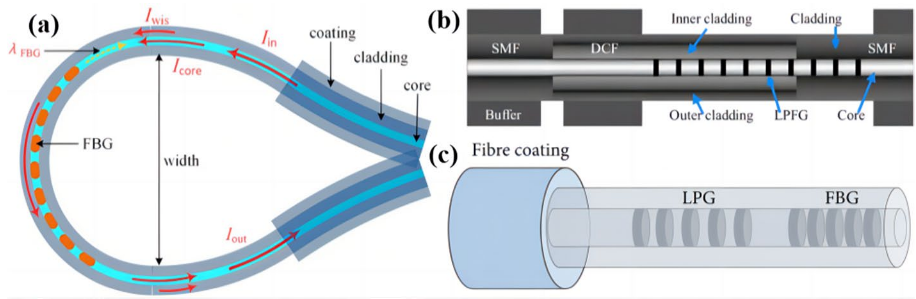

Fig. 5 Schematic diagram of gratings-based fiber interferometer sensors containing **a** bending FBG(Liu et al. 2016c) **b** separated LPFG(Han et al. 2012) **c** cascaded-LPFG-FBG(Berrettoni et al. 2015)

As shown in Fig. 5b, LPFG was part-etched to build two cascade-regions in a double-cladding fiber (DCF)(Han et al. 2012). Where, the exposing part is sensitive to both temperature and surrounding RI, while the cladding projecting part in DCF is only sensitive to temperature. TFBG can reflect part of the optical signal from the fiber core into the cladding layer. The corresponding reflection spectrum has the complex resonance multi-peak and multi-envelope, including the cladding/core mode components spectra(Alberto et al. 2011). The resonance coupling between the forward- and backward-propagating fiber core modes is temperature-dependent but free for RI, while the resonance coupling between the forward-propagating modes and the various back-propagating cladding modes exhibits a strong-depending relationship on either the surrounding RI or temperature. Generally, by monitoring the characteristic wavelength position of the core modes and the envelope area of the transmission spectrum, both RI and temperature can be measured. Figure 5c shows a cascade-LPFG-FBG composite structure in a single SMF(Berrettoni et al. 2015), whose characteristic wavelength are separately demodulated from the transmission and reflection spectra. In the similar fiber sensing structures, FBG was replaced by TFBG and be demonstrated for its dual-parameter sensing performance(Fan et al. 2019; Wong et al. 2011). Because its capability for exciting cladding modes, LPFG pairs can be used to construct the MZIs, where the light beams are split and transmit in the core modes and cladding modes to produce the interference spectra(Lu et al. 2014).

Other kinds of special fibers, such as CLF, was cascade-spliced with LPFGs to explore the dual-parameter sensor for measuring RI and temperature(Zhang et al. 2018). Where, the cladding modes was produced in the CLF and sensing the environmental RI. The LPFGs etched on the fiber core realize the coupling interference of the cladding modes and the core modes. RI increasing outside the optical fiber results that more cladding modes are leaked into the environment, thereby reducing the light intensity of interference spectrum. The RI and temperature response characteristics are obtained by demodulating the intensity and wavelength changes of the transmission interference spectrum, respectively. The sensitivity coefficient matrix can be constructed by cascaded-connect two LPFGs with different periods and demodulating the intensity and phase of the two corresponding characteristic wavelengths(Jiang et al. 2022b). The gratings with the same period have the same characteristic wavelength, which is equivalent to place a reflector mirror in the optical fiber to produce the multi-mode interference effect. LPFGs with different periods can be used as different sensing units. Each one can sensing the RI and temperature at the same time. The measuring parameters can be demodulated from the phase shift of the characteristic wavelength for different grating structures.

Compared with LPFGs, the FBGs with more stable structures play a more important role: (1) They were used as mirrors of special wavelength to construct the reflected fiber probe; (2) The reflected intensity near the characteristic wavelength changes with the phase shift of the interference spectrum, which can be used for the temperature compensation(Shi et al. 2017); (3) They can be pair-used to double-increase the temperature sensitivity based on the different shift directions for the different characteristic wavelengths under the temperature influence. The highly sensitive measuring for the environmental RI can be achieved by combining micro/nanofibers with FBG structures.

According to the coupling characteristics of the core modes in FBG and the cladding modes in LPFG, different grating structures can be combined to develop novel interferometers (FPI or MZI). By demodulating the intensity and phase information of the reflected or transmitted spectrum, the depending relationship to the ambient RI or temperature will be established. In this way, different measuring information are separately monitored in the different interference spectra. The FBGs with different periods were connected at the tail of a bending fiber loop to explore the high-performance dual-parameter fiber sensor for RI and temperature(Du et al. 2019). When a micro/nanofiber FBG is embedded in the SI ring(Cao et al. 2019), the positive correlation of its transmission spectral intensity varies with the external RI, resulting the high sensitivity of −744.6 dB/RIU. Some special fibers or micro/nano-processing method have been reported to optimize the sensing performance of the gratings based dual-parameter fiber sensors. The gold film was coated on the biconical chirped FBG (stCFBG) structure(Ayupova et al. 2021) and the transition tapered microfiber, which were respectively used for measuring RI and temperature. stCFBG is only sensitive to temperature, similar to the conventional FBG structure(Tosi 2018). A symmetrical side-staggered V-shaped groove was further processed on a SMF-LPFG by a high-frequency CO_2 laser(Ma et al. 2022). This novel dual-formant LPFG is then heated and stretched by a fiber heating-tapering system. Furthermore, its fiber core was bent to the grooves on both sides. The sinusoidal core is closer to the external environment and exhibits the excellent modulation performance for RI measurement, which results in the high RI sensitivity of 620 nm/RIU.

4.2 Fiber gratings structures combination

By combining the advantages of different interferometers, the sensing performance and demodulation efficiency of the RI and temperature dual-parameter fiber sensors can be improved. The composite fiber sensors based on FPI-MZI or FPI-MI can simultaneously measure RI and temperature relying on the different interference mechanisms.

Different types of interferometers can be embedded in the ring structures for developing the composite interferometers sensors, such as optical fiber ring-mirrors (the light power is continuously attenuated after each time of the unidirectional cyclic transmission) and SI (the phase difference is generated during the clock-opposite propagation of the light beams). The SI temperature and MZI RI sensing units can be cascaded within the same fiber system(Zhao et al. 2017b), as shown in Fig. 6a.

The working wavelength of SI can be adjusted by the fiber grating structure to effectively separate the measurement information for different parameters. Yuan et al. placed LPFBG before a SI and verified its detection capability for RI and temperature(Yuan et al. 2014), as shown in Fig. 6b. High sensitivity was achieved by means of strong evanescent field of micro/nanofibers. In addition, the micro/nanofiber knot resonators were

Fig. 6 Dual-parameter sensors structure combining SI with **a** bending fiber(Zhao et al. 2017b) and **b** LPFG(Yuan et al. 2014)

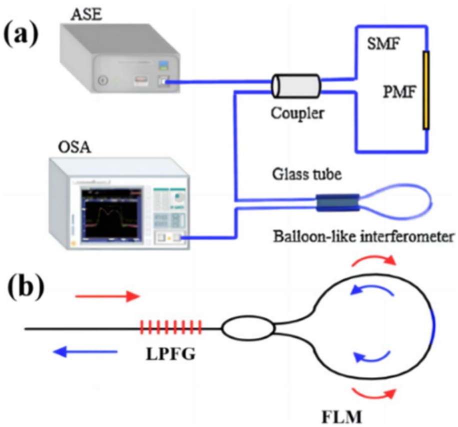

embedded in the high-birefringence fiber ring-mirrors for simultaneous measurement RI and temperature(Xiao et al. 2020). Although the above three structures response differently to RI and temperature, the relevant parameter information can be obtained by analyzing the sensitivity coefficient equations. The interference phase of SI is usually affected by the ambient temperature; while various composite fiber structures (usually including PMFs(Lu et al. 2018) and CLFs(Xiao et al. 2017), etc.) are highly sensitive to RI.

FBG supports the core-mode coupling and is usually used to build the miniature FPIs in the fiber core. Multi-interferometer is easily prepared in the same fiber structure. Two microporous structures with the same size was fabricated in the FBG region to construct the dual-FPI structure, which was verified with a good sensing performance for RI and temperature(Liu et al. 2018). Specifically, the air micropore FPI is sensitive to RI change; while the FBGs in the FP cavity is sensitive to temperature. RI and temperature can be measured respectively by monitoring the spectral envelope shift of the two FPIs and the characteristic wavelength shift of the FBG. In Fig. 7a, two FBGs were etched on both sides of the double-tapered micro/nanofiber to serve as two reflected mirrors of a micro-FPI(Xiang et al. 2018). The shift of the FPI phase and FBG characteristic wavelength on the reflection spectrum reveal the corresponding changes of RI and temperature, respectively. The spectrum envelope and resonance wavelengths were used to realize the dual-parameter measurement for RI and temperature. Organic polymer PDMS can also be used to prepare FPI for dual-parameter measurement(Zhu et al. 2022), as shown in Fig. 7b. This structure combines a PDMS-coated MZI with a TFBG. The cut-off mode of TFBG is used for sensing RI, which can effectively eliminate the temperature crosstalk.

Among the interferometer sensors with different structures, the mode field mismatched MZI sensor is designed by cascade-splicing various fibers with different mode fields. One can introduce FBG in either its sensing area or input/output end. The former one mainly provides the ambient temperature compensation, where the original sensing probe is generally only sensitive to RI, including TCFs(Zhou et al. 2017; Jiang et al. 2017) (Fig. 7c), micro/nanofibers(Ahmed et al. 2016), etc.; for the latter one, the main

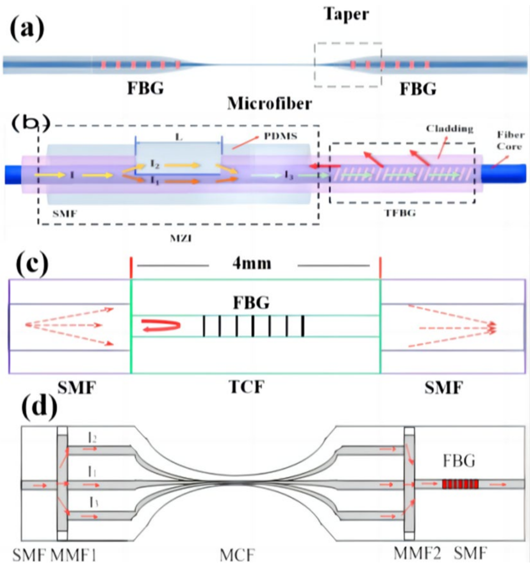

Fig. 7 Composition structures by fiber gratings and FPI based on **a** double-tapered micro/nanofiber(Xiang et al. 2018) **b** PDMS(Zhu et al. 2022) **c** FCF(Jiang et al. 2017) and **d** MCF(Zhang et al. 2021)

function is to introduce a reference wavelength into the interference spectrum to facilitate the signal demodulation process. These dual-parameter fiber sensors include the CLFs(Zhang et al. 2017), cascaded-MMF-MCF(Zhang et al. 2021) (Fig. 7d), cascaded-FCF-MMF(Li et al. 2021) and FMF(Li et al. 2019).

In an all-fiber MZI RI and temperature sensor, a dislocation-splicing structure was employed to excite the cladding modes and a diameter-raised cone structure to facilitate the coupling between the cladding and core modes(Cao et al. 2015a). The FBG for temperature compensation is prepared in the fiber core of output SMF, in which the optical signals with different wavelengths can propagate independently. The FBG in either the fiber core of the sensing area or the input/output SMF can sense the ambient temperature, so as to realize the temperature compensation and eliminate its cross-sensitivity effect(Yu et al. 2015). In contrast, to obtain the coupled resonance peak of the cladding modes in the transmission spectrum, a LPFG can be used instead of FBG in the input/output SMF(Cao et al. 2015b).

Either LPFG or FBG can be written in the input/output SMF part of the biconical dual-parameter sensing unit to construct an independent sensing probe and obtain the relevant characteristic wavelength in the transmission spectrum and reflection spectrum, respectively. Their difference lies in that the LPFG is sensitive to both RI and temperature, while the FBG is only sensitive to temperature changes. For example, U-shaped fiber was cascaded with FBG to prepare a bending fiber RI sensor with temperature compensation(Gong et al. 2017), as shown in Fig. 8a.

Similar fiber structures include the balloon-shape cascade-FBGs(Chen et al. 2015b), droplet-shape cascade-LPFGs(Zhu et al. 2021) and bending-core biased coaxial MZI(Wu et al. 2021) and so on. A section of LPFG was cascaded to the S-shape biconical micro/nanofiber(Li et al. 2013), as shown in Fig. 8b. Since the different RI and temperature sensitivities, the crosstalk between two-parameter measurements has been eliminated. Two trapezoidal pyramid structures have been connected to measure the ambient RI and temperature, in which the FBG was introduced to construct a two-parameter sensitivity coefficient matrix(Zhang et al. 2020) (Table 3).

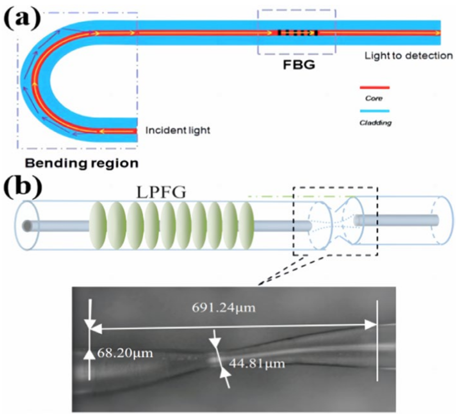

Fig. 8 Gratings and MZI/MI composite structures based on **a** bending fiber(Gong et al. 2017) and **b** and S-shape micro/nanofiber taper(Li et al. 2013)

Table 3 Performance comparison of optical fiber interferometers based on grating reflectors

RI sensitivity (nm/RIU)	Temperature sensitivity (pm/℃)	RI range (RIU)	T range (℃)	Refs.
218.56	−1700	1.3411–1.3819	50–63	61
113.142	153.3	1.333–1.430	20–50	62
116	464.1	1.3472–1.3490	30–40	63
131.49	1804	1.3376–1.3618	10–30	64
235.3	1929	1.3333–1.4280	1.2–49.8	65
1128.19	175	1.3345–1.3470	30–85	66
129.28–151.61	9.35–11.08	1.3–1.4	28–75	67
521.92	5150	1.333–1.3614	20–60	68
6.75	74.2	1.3333–1.3365	20–100	69
−58.13	51.1	1.384–1.420	30–75	70
126.1	67.4	1.33–1.40	25–95	71
399.20718	10.73	1.333–1.419	26.4–100	72
847	−31.43	1.3329–1.3357	27–62	73
−3244.22/14296.23	35.18	1.3409 −1.3347	30–70	74
794	−57.9	1.3164–1.3176	24–30	75
−91.76667	71.75	1.33–1.38	25–75	76
−26.22	46.5	1.3333–1.3925	20–100	77
−55.06	60.7	1.33–1.38	25–75	78
160	−85.6	1.3288–1.3730	30–50	79
157.8891	10.3	1.3330–1.3785	20–100	80
165.04	255.52	1.335–1.38	35–80	81
−115.5646	117.45	1.333–1.373	25–60	82
311.48	45.87	1.33–1.37	20–80	83
101.3	100	1.333–1.365	25–95	84

5 Separating multi-region based on film layer and special structures

By rationally distributing the working wavelength range, multiple sensing regions can be series-connected within a single fiber system, to simultaneously measure the different target parameters. In addition, the same probe can also be parallel-connected as the sensing optical path and the reference optical path, so as to effectively avoid the influence of the environmental fluctuations, and improve the detection accuracy(Peng et al. 2005). Therefore, the RI and temperature measurement can be obtained respectively in two separating sensing channels. Different sensitive materials or fiber components can be introduced to generate the two sensing channels for measuring RI and temperature.

Sensitive materials can convert the parameters changes into the forms of volume expanding, local heating, coloring, etc. Therefore, optical fiber sensors can indirectly measure the various physical and biochemical parameters through the equivalent RI changes, such as vibration, pressure, temperature, concentration, and composition. A sensing region can be selectively divided into different parts, so as to realize the selective detection of multiple parameters, similar to the cascade-sensors with the same mechanism. PDMS is one of the most commonly used temperature-sensitive materials, and has been reported in many works to improve the temperature sensitivity depending on its thermal expansion

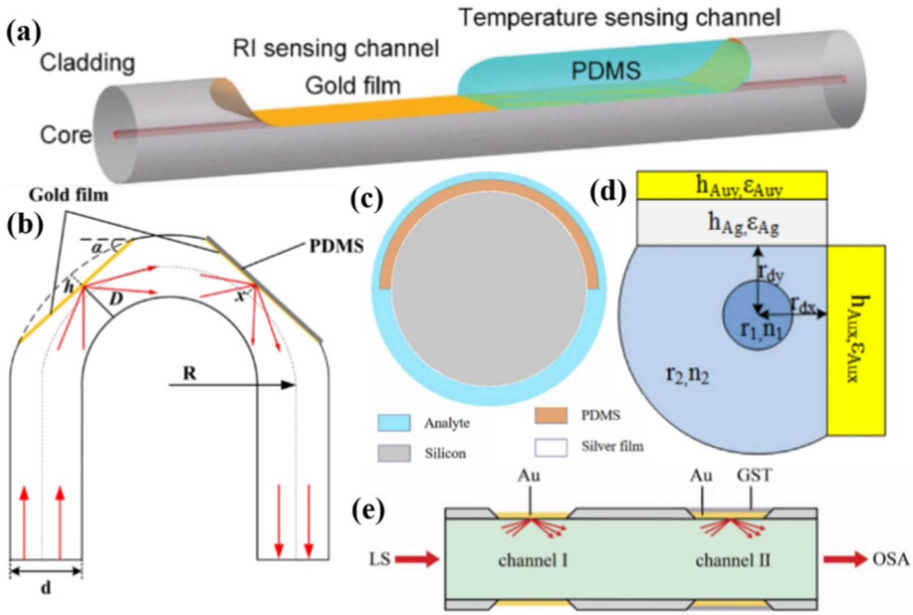

Fig. 9 Dual-channel fiber structures based on **a** Cascaded HCF-PCF(Zhao et al. 2016) **b** Cascaded PCF-MMF(Zhang et al. 2019), as well as the **c** C-shape open cavity(Luan et al. 2016) **d** D-shape side-polished(Zhao et al. 2019) and **e** twin-core PCF(Yin et al. 2022b)

Table 4 Performance comparison of multi-zone separation based on thin film layers and special structures

RI sensitivity (nm/RIU)	Temperature sensitivity (pm/℃)	RI range (RIU)	T range (℃)	Refs
2260.1	−2410	1.333–1.390	20–60	86
1258	−596	1.34–1.37	30–80	87
5200	7200	1.35–1.39	−50–200	88
2323.4	−2861	1.346–1.388	20–60	89
561.4286	47.36	1.2–1.4	10–70	90
5226	5880	1.333 – 1.403	25–70	91
178.7	454	1.33–1.37	20–80	92
−102,048.3 a.u/RIU	13	1.33–1.38	35–500	93
9.14 (dB/RIU)	11.46	1.332–1.3708	30–120	96
61.74 (dB/RI)	15	1.332–1.45	24–95	97
−30.82/171.96	47.4/10.4	1.33–1.3737	25–100	98
10,300	4220	1.41–1.42	−3–15	100
4520	4830	1.35–1.40	20–60	101
4000	30	1.30–1.38	26–43	102
20,000	9200	1.36–1.42	0–50	103

and thermo-optic effect. A dual-channel SPR sensor was constructed by coating PDMS on the SPR optical fiber. Where, the PDMS-coated part isolates the fluid to be measured from the optical signal and is only sensitive to temperature and reduce the crosstalk effect. For example, a D-shape fiber SPR RI sensor with temperature compensation was proposed(Liu et al. 2021), as shown in Fig. 9a, (Table 4).

The gold and PDMS film are coated on the polished D-surface to separate the RI and temperature monitoring area. The separated sensing regions can also be accomplished by the double-sided polished U-shaped plastic optical fiber (POF), which has been demonstrated for simultaneous measuring RI and temperature(Teng et al. 2022), as shown in Fig. 9b. The dual-parameter sensor can be obtained by coating a layer of PDMS film on one of the gold-film surfaces. The RI and temperature can be detected with the sensitivities of 1258 nm/RIU and − 0.596 nm/℃, respectively, by monitoring the resonance peak wavelength changes.

To effectively distinguish the SPR resonance wavelengths of different sensing units, different types or thicknesses of noble metal films were used(Yin et al. 2022a), as shown in Fig. 9c. In terms of low cost, a SMF can be spliced between two MMFs as the sensing region. Then, the metal nanofilms and PDMS was added(Velázquez-González et al. 2017). The corresponding RI and temperature sensitivity are quite high as 2323.4 nm/RIU and − 2861 pm/℃, respectively. In addition to sensitive materials, dual-parameter measurement can also be achieved by including the temperature-sensitive structures (such as gratings), or constructing an additional sensing channel (such as double D-shape fibers in (Fig. 9dWeng et al. 2016)).

Recently, an MZI cascaded dual-channel fiber sensor was proposed based on the phase-change material $Ge_2Sb_2Te_5$(Zhang et al. 2022a), as shown in Fig. 9e. This material moves the working range of SPR to the infrared band, thereby perfectly distinguishing the phase change information of RI (596 ~ 793 nm) and temperature (1045 ~ 1421 nm) in the transmission spectrum. The sensitivity of Channel l (596–793 nm) reaches 2781 nm/RIU. The sensitivity of Channel II (1045–1421 nm) reaches 5226 nm/RIU.

Dual-channel sensors can be designed by constructing two sensing regions inside or outside the PCF, respectively. In PCF-based RI sensors, the radially penetrating micro-air array will be used as the RI detection channel, but the measured object is generally limited to gas. When it is used for liquid RI detection, the length of the PCF will be severely limited. Furthermore, it is necessary to fabricate the flow-conducting micropores to improve the exchanging efficient of analyte liquid. By filling the air micro-holes with the high-RI temperature-sensitive liquid, it will be directionally coupled with the fiber core modes and become sensitive to ambient temperature changes.

Furthermore, the sensing information can be obtained from the reflected and transmitted light beam of the composite interferometer, respectively, so as to avoid the superposition of multiple interference spectra. The interference spectrum for each sensing unit can be acquired independently, which effectively reduces the crosstalk during the multi-parameter measurement. A length of HCF and PCF were inserted into a SMF system(Zhao et al. 2016), as shown in Fig. 10a. Where, the FPI temperature unit contains an HCF filled by alcohol with high thermal coefficient; the MZI RI measurement region is composited by the HCF and PCF, relying on the interference effect between the core and the cladding modes. The similar cascaded composite structures can be realized with special fiber devices, such as couplers or circulators. For example, a fiber coupler-based FPI/MI composite sensor was reported for simultaneous measurement of RI and temperature(Sun et al. 2013). The two output SMFs were cut into different lengths to construct the 2 × 2 coupler of one MI, whose interference phase is dependent on the RI change near the end

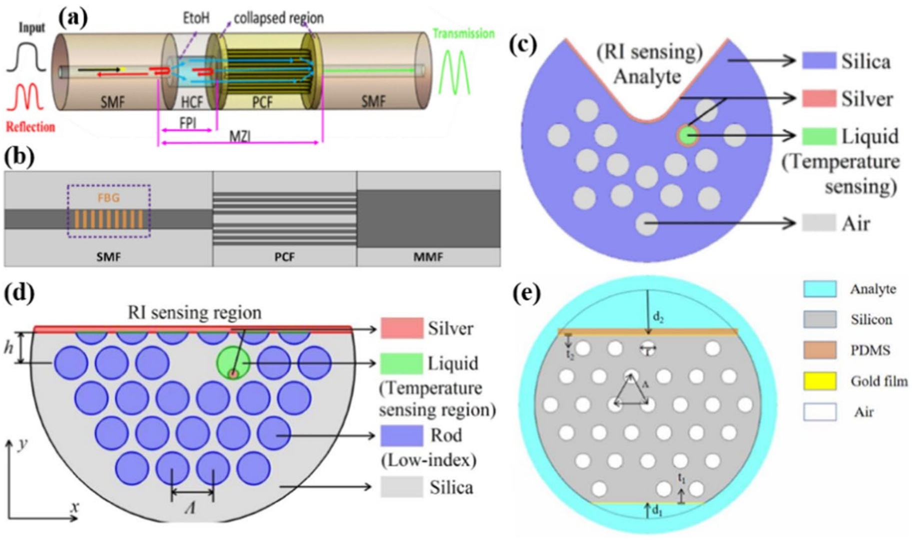

Fig. 10 PDMS-based fiber structures including **a** D-shape fiber(Liu et al. 2021) **b** double-polished U-shape(Teng et al. 2022), **c** differential design of metal layer(Yin et al. 2022a) **d** double-polished fiber(Weng et al. 2016) and **e** phase-change material $Ge_2Sb_2Te_5$(Zhang et al. 2022a)

face of SMFs; furthermore, a section of PCF was spliced on one of the SMFs for sensing ambient temperature. Although a single microfiber coupler has also been used for simultaneous monitoring RI and temperature, the measurement is achieved by demodulating the accumulated phase difference between odd and even modes in the tapered transition region(Bilodeau et al. 1987; Yang et al. 1998). The corresponding transmission spectra are superimposed and cluttered, requiring the complex demodulation algorithms to resolve the phase change information.

The FPI is easy to obtained by cascade-splicing different fibers, including PCF. The PCF and MMF based FPI was reported and realized the real-time monitoring of the fluid RI with the help of the natural air micropores of PCF (PCF containing multi-layer air micropores, resulting its free-dependence for temperature changes). Furthermore, the FBG was etched on the SMF's core to sense the ambient temperature(Zhang et al. 2019), as shown in Fig. 10b. Similarly, SMF and PCF with an air chamber(Wang and Wang 2012) or microbubble(Hu et al. 2012) was cascaded to construct an FPI. Then, the nanometer-thick of noble metal film layer was modified on the corresponding processed surface to stimulate the SPR effect. The exposed core PCF-SPR structure(Luan et al. 2016) and the solid D-shape PCF sensor(Zhao et al. 2019) for simultaneous measurement of RI and temperature are shown in Fig. 10c, d, respectively. The coating layer of silver nanofilms have been widely used for sensing RI(Zhang et al. 2022b). Meanwhile, the air micro-holes are selectively filled with temperature-sensitive liquids. The outer surface or inner holes can be further elaborated by silver nanofilms and silver nanowires The D-shape PCF dual-parameter sensor was filled with gold nanowires(Santos et al. 2017). It combined the temperature-sensitive materials and noble metal nanostructures to build the two sensing channels and produce the two orthogonally polarized independent resonance peaks on the transmission spectra. The RI and temperature sensitivities were experimentally demonstrated to be 4000 nm/RIU and 30 pm/℃, respectively. A twin-core PCF sensor is proposed for measuring liquid RI and temperature simultaneously(Yin et al. 2022b), as shown in Fig. 10e. Where, the air holes of PCF are arranged in a hexagonal pattern, and two planes are introduced by polishing the cladding layer. On one side of the plane, the gold film was deposited for RI measurement, and on the other side, the gold film and PDMS were deposited for temperature measurement.

Multi-region separation techniques based on thin film layers and special structures have the advantages of high sensitivity and versatility. It can measure two different parameters simultaneously, providing more comprehensive information. However, the preparation and operation of this technology is relatively complex, there may be cross-interference problems, and the scope of application is limited. Therefore, in practical applications, these factors need to be considered comprehensively, and selected and optimized according to specific needs.

6 Conclusions and perspectives

This paper reviews the compact dual-parameter fiber sensors for measuring RI and temperature simultaneously and independent. The design methods and working principles are reasonable classified, and their corresponding sensing performances are compared. The typical interferometer structures based on different fiber interferometers and gratings used to realize the RI and temperature dual-parameter sensing have been detailed analyzed and discussed, which includes various forms of interferometer fiber sensors based on the mode field mismatch-splicing, fiber core dislocation-splicing, diameter abruption, U-shape bending, and gratings. However, in such sensors, the sensing regions for RI and temperature will overlap usually and exert the serious impact on the sensitivity and accuracy. By series-connecting a temperature-sensitive FBG, the temperature crosstalk effect can be greatly reduced to improve the measurement accuracy. For the target details, as well as their surrounding environment and performance requirements, different types of multi-parameter fiber sensors need to be reasonably selected and optimized, including their structures, fiber types, sensitive materials, and surface structures.

The RI and temperature fiber optic sensors have been witnessed with the significant advancements through their applications in the detection of various chemical and physical parameters. The composite interferometers should be paid more attentions for their unique properties and high performance. The dual parameters simultaneously measurement usually requires a high contrast spectrum. The mutual influence between different parameters is difficult to solve for the simple structure. Therefore, the research on the composite interference has been increasing in recent years. The measuring information for different parameters are separated by some special designs during the measurement process, where the sensing crosstalk is reduced. However, the sensitivity is seriously limited by the nature of the optical fiber. Novel techniques, materials or fiber structures will be introduced to develop some miniature multi-parameter fiber sensors with more stability and sensitivity.

Author contributions CD, KZ and MT collected and review references; CD wrote original draft; JL checked and revised manuscript. All authors have approved this manuscript.

Funding This work was supported by the National Key R&D Program of China (2019YFB2006001).

Data availability The data or materials can be requested from the authors.

Declarations

Conflict of interest No author has financial or other contractual agreements that might cause conflicts of interest.

Ethical approval Not applicable.

References

Ahmed, F., Ahsani, V., Saad, A., et al.: Bragg grating embedded in Mach-Zehnder interferometer for refractive index and temperature sensing[J]. IEEE Photonics Technol. Lett. **28**(18), 1968–1971 (2016)

Alberto N J, Marques C A, Pinto J L, et al. (2011) Simultaneous temperature and refractive index sensor based on a tilted fibre Bragg grating[C]. In: International Conference on Applications of Optics and Photonics. SPIE, 8001: 576–582.

Ayupova, T., Shaimerdenova, M., Tosi, D.: Shallow-tapered chirped fiber Bragg grating sensors for dual refractive index and temperature sensing[J]. Sensors **21**(11), 3635 (2021)

Bernier, M., Trépanier, F., Carrier, J., et al.: High mechanical strength fiber Bragg gratings made with infrared femtosecond pulses and a phase mask[J]. Opt. Lett. **39**(12), 3646–3649 (2014)

Berrettoni, C., Trono, C., Vignoli, V., et al.: Fibre tip sensor with embedded FBG-LPG for temperature and refractive index determination by means of the simple measurement of the FBG characteristics[J]. J. Sens. **2015**, 491391 (2015)

Bilodeau, F., Hill, K.O., Johnson, D.C., et al.: Compact, low-loss, fused biconical taper couplers: overcoupled operation and antisymmetric supermode cutoff[J]. Opt. Lett. **12**(8), 634–636 (1987)

Cao, Y., Zhao, C., Tong, Z.: All fiber sensor based on Mach-Zehnder interferometer for simultaneous measurement of temperature and refractive index[J]. Optoelectron. Lett. **11**(6), 438–443 (2015a)

Cao, Y., Liu, H., Tong, Z., et al.: Simultaneous measurement of temperature and refractive index based on a core-offset Mach-Zehnder interferometer cascaded with a long-period fiber grating[J]. Optoelectron. Lett. **11**(1), 69–72 (2015b)

Cao, Y., Zhang, H., Miao, Y., et al.: Simultaneous measurement of temperature and refractive index based on microfiber Bragg Grating in Sagnac loop[J]. Opt. Fiber Technol. **47**, 147–151 (2019)

Chen, Y., Wang, Y., Chen, R., et al.: A hybrid multimode interference structure-based refractive index and temperature fiber sensor[J]. IEEE Sens. J. **16**(2), 331–335 (2015a)

Chen, Y., Han, Q., Liu, T., et al.: Simultaneous measurement of refractive index and temperature using a cascaded FBG/droplet-like fiber structure[J]. IEEE Sens. J. **15**(11), 6432–6436 (2015b)

Du, Y., Han, Q., Hu, H., et al.: High-sensitivity refractive index and temperature sensor based on cascading FBGs and droplet-like fiber interferometer[J]. Sens. Actuators, A **299**, 111631 (2019)

Fan, X., Jiang, J., Zhang, X., et al.: Simultaneous measurement of refractive index and temperature using a hybrid-grating sensor[J]. Appl. Phys. Express **12**(11), 116501 (2019)

Flores-Bravo, J.A., Fernández, R., Lopez, E.A., et al.: Simultaneous sensing of refractive index and temperature with supermode interference[J]. J. Lightwave Technol. **39**(22), 7351–7357 (2021)

Fu, X., Liu, L., Huang, S., et al.: Simultaneous measurement of temperature and refractive index with F-P microcavity sensor based on graded-index few mode fiber[J]. Opt. Commun. **455**, 124577 (2020)

Ge, J., Zhang, Y., Zhang, W., et al.: Simultaneous measurement of RI and temperature based on compact U-shaped interferometer[J]. IEEE Sens. J. **20**(7), 3593–3598 (2020)

Gong, Z., Chen, K., Zhou, X., et al.: Temperature-compensated refractive index sensor based on bent-fiber interference[J]. Opt. Fiber Technol. **36**, 6–9 (2017)

Gunawardena Serandi, D., Ahmad, H., et al.: Cladless few mode fiber grating sensor for simultaneous refractive index and temperature measurement[J]. Sens. Actuators A Phys. **228**, 62–68 (2015)

Guo, L.N., Li, J., Meng, F.L.: Refractive index sensing performance of stepped-mTFBG fabricated by flexibly-regulating wet etching process[J]. Sens. Actuators, A **346**, 113875 (2022a)

Guo, L.N., Li, J., Meng, F.L.: Refractive index sensing performance of stepped-mTFBG fabricated by flexibly-regulating wet etching process[J]. Sens. Actuators a: Phys. **346**, 113875 (2022b)

Han, Q., Lan, X., Huang, J., et al.: Long-period grating inscribed on concatenated double-clad and single-clad fiber for simultaneous measurement of temperature and refractive index[J]. IEEE Photonics Technol. Lett. **24**(13), 1130–1132 (2012)

Hu, D.J.J., Lim, J.L., Jiang, M., et al.: Long period grating cascaded to photonic crystal fiber modal interferometer for simultaneous measurement of temperature and refractive index[J]. Opt. Lett. **37**(12), 2283–2285 (2012)
Hu, T., Zhao, Y., Song, A.N.: Fiber optic SPR sensor for refractive index and temperature measurement based on MMF-FBG-MMF structure. Sens. Actuators, B Chem. **237**, 521–525 (2016)
Hu, Y., Lin, Q., Yan, F., et al.: Simultaneous measurement of the refractive index and temperature based on a hybrid fiber interferometer[J]. IEEE Sens. J. **20**(22), 13411–13417 (2020)
Jiang, M., Wang, Z.M., Zhao, Z.Z., et al.: Long-period fiber grating cascaded to thin-core fiber for simultaneous measurement of liquid refractive-index and temperature[J]. Sensor Rev. **38**(1), 79–83 (2017)
Jiang, Z., Wu, F., Yang, J., et al.: Combined-Vernier effect based on hybrid fiber interferometers for ultrasensitive temperature and refractive index sensing[J]. Opt. Express **30**(6), 9578–9589 (2022a)
Jiang, H., Gu, Z., Gao, K., et al.: A high sensitivity sensor based on novel CLPFG with wavelength and intensity modulation for simultaneous measurement of SRI and temperature[J]. Opt. Fiber Technol. **70**, 102886 (2022b)
Lacraz, A., Polis, M., Theodosiou, A., et al.: Femtosecond laser inscribed Bragg gratings in low loss CYTOP polymer optical fiber[J]. IEEE Photonics Technol. Lett. **27**(7), 693–696 (2015)
Li, J., Zhang, W., Gao, S., et al.: Long-period fiber grating cascaded to an S fiber taper for simultaneous measurement of temperature and refractive index[J]. IEEE Photonics Technol. Lett. **25**(9), 888–891 (2013)
Li, X., Nguyen, L.V., Becker, M., et al.: Simultaneous measurement of temperature and refractive index using an exposed core microstructured optical fiber[J]. IEEE J. Sel. Top. Quantum Electron. **26**(4), 1–7 (2019)
Li, X.G., Warren-Smith, S.C., Xie, L., et al.: Temperature-compensated refractive index measurement using a dual Fabry-Perot interferometer based on C-fiber cavity[J]. IEEE Sens. J. **20**(12), 6408–6413 (2020)
Li, J., Gan, W., Li, H., et al.: Temperature compensated highly sensitive refractive index sensor based on Mach-Zehnder interferometer and FBG[J]. Optik **241**, 166838 (2021)
Li, J., Chen, G.L., Meng, F.L.: A fiber-optic formic acid gas sensor based on molybdenum disulfide nanosheets and chitosan works at room temperature[J]. Opt. Laser Technol. **150**, 107975 (2022)
Liu, J., Wang, D.N., Zhang, L.: Slightly tapered optical fiber with dual inner air-cavities for simultaneous refractive index and temperature measurement[J]. J. Lightwave Technol. **34**(21), 4872–4876 (2016a)
Liu, S., Tian, J., Liu, N., et al.: Temperature insensitive liquid level sensor based on antiresonant reflecting guidance in silica tube[J]. J. Lightwave Technol. **34**(22), 5239–5243 (2016b)
Liu, T., Chen, Y., Han, Q., et al.: Sensor based on macrobent fiber Bragg grating structure for simultaneous measurement of refractive index and temperature[J]. Appl. Opt. **55**(4), 791–795 (2016c)
Liu, Y., Liu, X., Ma, C., et al.: Micro-structured optical fiber sensor for simultaneous measurement of temperature and refractive index[J]. Opt. Fiber Technol. **41**, 168–172 (2018)
Liu, W., Wu, X., Zhang, G., et al.: Refractive index and temperature sensor based on Mach-Zehnder interferometer with thin fibers[J]. Opt. Fiber Technol. **54**, 102101 (2020)
Liu, L., Liu, Z., Zhang, Y., et al.: Side-polished D-type fiber SPR sensor for RI sensing with temperature compensation[J]. IEEE Sens. J. **21**(15), 16621–16628 (2021)
Lu, Y., Shen, C., Zhong, C., et al.: Refractive index and temperature sensor based on double-pass M-Z interferometer with an FBG[J]. IEEE Photonics Technol. Lett. **26**(11), 1124–1127 (2014)
Lu, H., Yue, Y., Du, J., et al.: Temperature and liquid refractive index sensor using PD fiber structure-based Sagnac loop[J]. Opt. Express **26**(15), 18920–18927 (2018)
Lu, P., Lalam, N., Badar, M., et al.: Distributed optical fiber sensing: Review and perspective[J]. Appl. Phys. Rev. **6**(4), 041302 (2019)
Luan, N., Ding, C., Yao, J.: A refractive index and temperature sensor based on surface plasmon resonance in an exposed-core microstructured optical fiber[J]. IEEE Photonics J. **8**(2), 1–8 (2016)
Luo, H., Sun, Q., Xu, Z., et al.: Microfiber-based inline Mach-Zehnder interferometer for dual-parameter measurement[J]. IEEE Photonics J. **7**(2), 1–8 (2015)
Ma, Y., Su, C., Dai, Z., et al.: Sinusoidal-core long period fiber grating for refractive index measurement[J]. J. Lightwave Technol. **40**(14), 4903–4910 (2022)
Mohammed, W.S., Mehta, A., Johnson, E.G.: Wavelength tunable fiber lens based on multimode interference[J]. J. Lightwave Technol. **22**(2), 469 (2004)
Ni, X., Ming, W., Guo, D., et al.: A hybrid mach-zehnder interferometer for refractive index and temperature measurement[J]. IEEE Photonics Technol. Lett. **28**(17), 1850–1853 (2016a)
Ni, X.L., Fu, S.N., Zhao, Z.Y.: Thin-fiber-based Fabry-Pérot cavity for monitoring microfluidic refractive index[J]. IEEE Photonics J. **8**(3), 1–7 (2016b)
Ouyang, Y., Xu, X., Zhao, Y., et al.: Temperature compensated refractometer based on parallel fiber Fabry-Pérot interferometers[J]. IEEE Photonics Technol. Lett. **30**(13), 1262–1265 (2018)

Peng, W., Banerji, S., Kim, Y.C., et al.: Investigation of dual-channel fiber-optic surface plasmon resonance sensing for biological applications[J]. Opt. Lett. **30**(22), 2988–2990 (2005)
Pevec, S., Donlagic, D.: High resolution, all-fiber, micro-machined sensor for simultaneous measurement of refractive index and temperature[J]. Opt. Express **22**(13), 16241–16253 (2014)
Ran, Z., Li, C., Zuo, H., et al.: Laser-machined cascaded micro cavities for simultaneous measurement of dual parameters under high temperature[J]. IEEE Sens. J. **13**(5), 1988–1991 (2013)
Santos, D.F., Guerreiro, A., Baptista, J.M.: Simultaneous plasmonic measurement of refractive index and temperature based on a D-type fiber sensor with gold wires[J]. IEEE Sens. J. **17**(8), 2439–2446 (2017)
Sharma, A.K., Pandey, A.K., Kaur, B.: A review of advancements (2007–2017) in plasmonics-based optical fiber sensors[J]. Opt. Fiber Technol. **43**, 20–34 (2018)
Shi, J., Wang, Y., Xu, D., et al.: Temperature self-compensation high-resolution refractive index sensor based on fiber ring laser[J]. IEEE Photonics Technol. Lett. **29**(20), 1743–1746 (2017)
Shi F, Zhao C L, Xu B, et al. (2015) Simultaneous measurement of refractive index and temperature base on three-beam interferometric fiber-optic[C]. In: 2015 Optoelectronics Global Conference (OGC). IEEE, 1-3.
Su, J., Tong, Z., Cao, Y., et al.: Double-parameters optical fiber sensor based on spherical structure and multimode fiber[J]. IEEE Photonics Technol. Lett. **27**(4), 427–430 (2014)
Sun, H., Zhang, J., Rong, Q., et al.: A hybrid fiber interferometer for simultaneous refractive index and temperature measurements based on Fabry–Perot/Michelson interference[J]. IEEE Sens. J. **13**(5), 2039–2044 (2013)
Sun, W., Zhang, X., Yu, Y., et al.: Comparative study on transmission mechanisms in a SMF-capillary-SMF structure[J]. J. Lightwave Technol. **38**(15), 4075–4085 (2020)
Teng, C., Shao, P., Li, S., et al.: Double-side polished U-shape plastic optical fiber based SPR sensor for the simultaneous measurement of refractive index and temperature[J]. Opt. Commun. **525**, 128844 (2022)
Tong, Z., Su, J., Cao, Y., et al.: Simultaneous measurement based on composite interference structure[J]. IEEE Photonics Technol. Lett. **26**(13), 1310–1313 (2014)
Tong, Z., Zhong, Y., Xue, W., et al.: Research on simultaneous measurement of refractive index and temperature comprising few mode fiber and spherical structure[J]. Optics Communications **421**, 1–6 (2018)
Tosi, D.: Review of chirped fiber Bragg grating (CFBG) fiber-optic sensors and their applications[J]. Sensors **18**(7), 2147 (2018)
Velázquez-González, J.S., Monzón-Hernández, D., Moreno-Hernández, D., et al.: Simultaneous measurement of refractive index and temperature using a SPR-based fiber optic sensor[J]. Sens. Actuators, B Chem. **242**, 912–920 (2017)
Wang, R., Qiao, X.: Hybrid optical fiber Fabry-Perot interferometer for simultaneous measurement of gas refractive index and temperature[J]. Appl. Opt. **53**(32), 7724–7728 (2014)
Wang, T., Wang, M.: F-P fiber sensor for simultaneous measurement of refractive index and temperature based on an in-fiber ellipsoidal cavity[J]. IEEE Photonics Technol. Lett. **24**(19), 1733–1736 (2012)
Wang, H., Meng, H., Xiong, R., et al.: Simultaneous measurement of refractive index and temperature based on asymmetric structures modal interference[J]. Opt. Commun. **364**, 191–194 (2016)
Wang, K., Dong, X., Köhler, M.H., et al.: Advances in optical fiber sensors based on multimode interference (MMI): a review[J]. IEEE Sens. J. **21**(1), 132–142 (2020a)
Wang, F., Pang, K., Ma, T., et al.: Folded-tapered multimode-no-core fiber sensor for simultaneous measurement of refractive index and temperature[J]. Opt. Laser Technol. **130**, 106333 (2020b)
Weng, S., Pei, L., Liu, C., et al.: Double-side polished fiber SPR sensor for simultaneous temperature and refractive index measurement[J]. IEEE Photonics Technol. Lett. **28**(18), 1916–1919 (2016)
Wong, A.C.L., Chung, W.H., Tam, H.Y., et al.: Single tilted Bragg reflector fiber laser for simultaneous sensing of refractive index and temperature[J]. Opt. Express **19**(2), 409–414 (2011)
Wu, S., Yan, G., Zhou, B., et al.: Open-cavity Fabry-Perot interferometer based on etched side-hole fiber for microfluidic sensing[J]. IEEE Photonics Technol. Lett. **27**(17), 1813–1816 (2015)
Wu, B., Bao, H., Zhou, Y., et al.: Temperature dependence of a refractive index sensor based on a bent core-offset in-line fiber Mach-Zehnder interferometer[J]. Opt. Fiber Technol. **67**, 102748 (2021)
Xiang, Y., Luo, Y., Li, Y., et al.: Quasi-distributed dual-parameter optical fiber sensor based on cascaded microfiber Fabry-Perot interferometers[J]. IEEE Photonics J. **10**(2), 1–9 (2018)
Xiao, S., Wu, Y., Dong, Y., et al.: Simultaneous measurement of refractive index and temperature using SMP in Sagnac loop[J]. Opt. Laser Technol. **96**, 254–258 (2017)
Xiao, Y.Y., Zhu, Z.H., Jiang, X.Y., et al.: Simultaneous measurement of temperature and refractive index using microfiber knot resonators in Hi-Bi fiber loop mirrors[J]. Optik **219**, 165232 (2020)

Yang, S.W., Wu, T.L., Wu, C.W., et al.: Numerical modeling of weakly fused fiber-optic polarization beam splitters–part II: the three-dimensional electromagnetic model[J]. J. Lightwave Technol. **16**(4), 691 (1998)
Yao, Q.Q., Meng, H.Y., Wang, W., et al.: Simultaneous measurement of refractive index and temperature based on a core-offset Mach-Zehnder interferometer combined with a fiber Bragg grating[J]. Sens. Actuators, A **209**, 73–77 (2014)
Yin, Z., Jing, X., Zhang, H., et al.: Dual-parameter sensor for simultaneously measuring refractive index and temperature based on no-core fiber and SPR effect[J]. Optik **262**, 169320 (2022a)
Yin, Z., Jing, X., Feng, Y., et al.: Refractive index and temperature dual parameter sensor based on a twin-core photonic crystal fiber[J]. J. Phys. D Appl. Phys. **55**(15), 155108 (2022b)
Yu, X., Chen, X., Bu, D., et al.: In-fiber modal interferometer for simultaneous measurement of refractive index and temperature[J]. IEEE Photonics Technol. Lett. **28**(2), 189–192 (2015)
Yuan, J., Zhao, C.L., Zhou, Y., et al.: Reflective long-period fiber grating-based sensor with Sagnac fiber loop mirror for simultaneous measurement of refractive index and temperature[J]. Appl. Opt. **53**(29), H85–H90 (2014)
Zhang, X., Peng, W.: Bent-fiber intermodal interference based dual-channel fiber optic refractometer[J]. Opt. Express **23**(6), 7602–7610 (2015)
Zhang, X.Y., Yu, Y.S., Zhu, C.C., et al.: Miniature end-capped fiber sensor for refractive index and temperature measurement[J]. IEEE Photonics Technol. Lett. **26**(1), 7–10 (2013)
Zhang, C., Xu, S., Zhao, J., et al.: Multipoint refractive index and temperature fiber optic sensor based on cascaded no core fiber-fiber Bragg grating structures[J]. Opt. Eng. **56**(2), 027102 (2017)
Zhang, J., Pu, S., Rao, J., et al.: Refractive index and temperature sensors based on no-core fiber cascaded with long period fiber grating[J]. J. Mod. Opt. **65**(9), 1098–1103 (2018)
Zhang, W., Tuerdahong, N., Zhu, L., et al.: Temperature and refractive index measurement using an optical fiber sensor featuring PCF-FP and FBG inscribed by femtosecond laser[J]. Optik **194**, 163095 (2019)
Zhang, W., Gao, W., Tong, Z., et al.: Mach-Zehnder interferometer cascaded with FBG for simultaneous measurement of RI and temperature[J]. Optics Communications **466**, 125624 (2020)
Zhang, H., Cong, B., Zhang, F., et al.: Simultaneous measurement of refractive index and temperature by Mach-Zehnder cascaded with FBG sensor based on multi-core microfiber[J]. Opt. Commun. **493**, 126985 (2021)
Zhang, Y., Xue, J., Liu, W., et al.: Cascaded dual-channel fiber SPR sensor based on $Ge_2Sb_2Te_5$[J]. IEEE Sens. J. **22**(5), 4083–4089 (2022a)
Zhang, J., Yuan, J., Qu, Y., et al.: A surface plasmon resonance-based photonic crystal fiber sensor for simultaneously measuring the refractive index and temperature[J]. Polymers **14**(18), 3893 (2022b)
Zhao, Y., Cai, L., Li, X.G.: High sensitive modal interferometer for temperature and refractive index measurement[J]. IEEE Photonics Technol. Lett. **27**(12), 1341–1344 (2015)
Zhao, Y., Li, X.G., Cai, L., et al.: Measurement of RI and temperature using composite interferometer with hollow-core fiber and photonic crystal fiber[J]. IEEE Trans. Instrum. Meas. **65**(11), 2631–2636 (2016)
Zhao, R., Lang, T., Chen, J., et al.: Polarization-maintaining fiber sensor for simultaneous measurement of the temperature and refractive index[J]. Opt. Eng. **56**(5), 057113 (2017a)
Zhao, Y., Liu, X., Lv, R.Q., et al.: Simultaneous measurement of RI and temperature based on the combination of Sagnac loop mirror and balloon-like interferometer[J]. Sens. Actuators, B Chem. **243**, 800–805 (2017b)
Zhao, J., Niu, P., Zhang, C., et al.: Simultaneous refractive index and temperature measurement using nested fiber balloon rings[J]. Appl. Opt. **57**(23), 6835–6839 (2018)
Zhao, L., Han, H., Lian, Y., et al.: Theoretical analysis of all-solid D-type photonic crystal fiber based plasmonic sensor for refractive index and temperature sensing[J]. Opt. Fiber Technol. **50**, 165–171 (2019)
Zheng, J., Liu, B., Zhao, L., et al.: An optical sensor designed from cascaded anti-resonant reflection waveguide and fiber ring-shaped structure for simultaneous measurement of refractive index and temperature[J]. IEEE Photonics J. **14**(1), 1–6 (2022)
Zhou, C., Zhou, Q., He, C., et al.: Fiber optic sensor for simultaneous measurement of refractive index and temperature based on internal-and-external-cavity Fabry-Pérot interferometer configuration[J]. IEEE Sens. J. **21**(8), 9877–9884 (2021)
Zhou M, Dong X, Liu X. (2017) Simultaneous measurement of temperature and refractive index with thin-core fiber MZI containing fiber Bragg grating[C]. In: 2017 16th International Conference on Optical Communications and Networks (ICOCN). IEEE, 1–3.
Zhu, Y., Zheng, J., Deng, H., et al.: Refractive index and temperature measurement by cascading macrobending fiber and a sealed alternated SMF-MMF structure[J]. Opt. Commun. **485**, 126738 (2021)

Zhu, F., Hao, X., Zhang, Y., et al.: D-shaped optic fiber temperature and refractive index sensor assisted by tilted fiber bragg grating and PDMS film[J]. Sens. Actuators, A **346**, 113870 (2022)
Zuo, B.Z., Liang, X., Zhang, X.R., et al.: Detection of refractive index with a temperature-compensated MZI-based optical sensor using few-mode fiber[J]. IEEE Access **9**, 158651–158659 (2021)